

Chapter 2

Evaporative purification

↙ defined?

In order to study the effects of N , the first thing needed is to obtain monodisperse samples with different N values. This has been achieved through evaporative purification technique, which has been practiced on low molecular weight polystyrene, and proved to be an efficient way to obtain highly monodisperse polymers[8].

2.1 Vapor pressure of PEO oligomers

For a particular polymer

N ?

imprecise

As the size of a polymer decreases, its vapor pressure increases, and for polymers with small enough N values, they have vapor pressure that leads to a relatively fast evaporation at high temperatures. More importantly, smaller N 's evaporates faster due to higher vapor pressure. This fact potentially allows one to separate polymer components with different N values.

Simple idea
that molecules of different sizes have different vapor pressures
→ distillation

To examine the feasibility of separating components by taking advantage of the difference in their evaporation speed, it is a good idea to first look at their vapor pressures. Unfortunately, vapor pressure of pure PEO, or even other polymer melts, has rarely been measured directly. Therefore, we applied a theoretical model to calculate the vapor pressures of low molecular weight PEO.

Sanchez and Lacombe Lattice-Fluid Model[9] describes a fluid using only three molecular parameters, and provides a method to calculate the relation between vapor pressure and temperature for a given N value. These three parameters for PEO could be found in the literature[10].

In this model, Gibbs free energy G is a function of mass density ρ :

$$G = -\rho + P\rho + T[(\nu - 1) \ln(1 - \rho) + \frac{1}{r} \ln(\rho/\omega)] \quad (2.1)$$

where P is pressure, and T is temperature. For a specific N at given pressure and temperature, G could be plotted as a function of ρ as shown below.

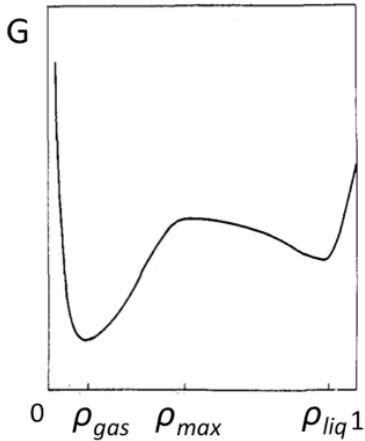


Figure 2.1: Gibbs free energy vs mass density, where a liquid phase is metastable with respect to the vapor phase.

The curve has two local minima. The first minimum represents gas phase, with lower mass density, and the second minimum represents liquid phase, with higher mass density. By tuning pressure or temperature, the two minima could be adjusted equal, which means the system takes equal probability to be in the state of gas or liquid. At a given temperature, there exists only one pressure that satisfies this equality, and this pressure and temperature are defined as the saturation pressure and temperature. The locus of all the saturation points represents the saturation/coexistence line, which is in fact the curve of vapor pressure with respect to temperature.

Solving for Equation 2.1 and applying the three molecular parameters found in literature, we were able to calculate the vapor pressure curve for each N value of PEO oligomers. The results are shown in the plot below, and note that each curve has been generated from 10-20 data points.

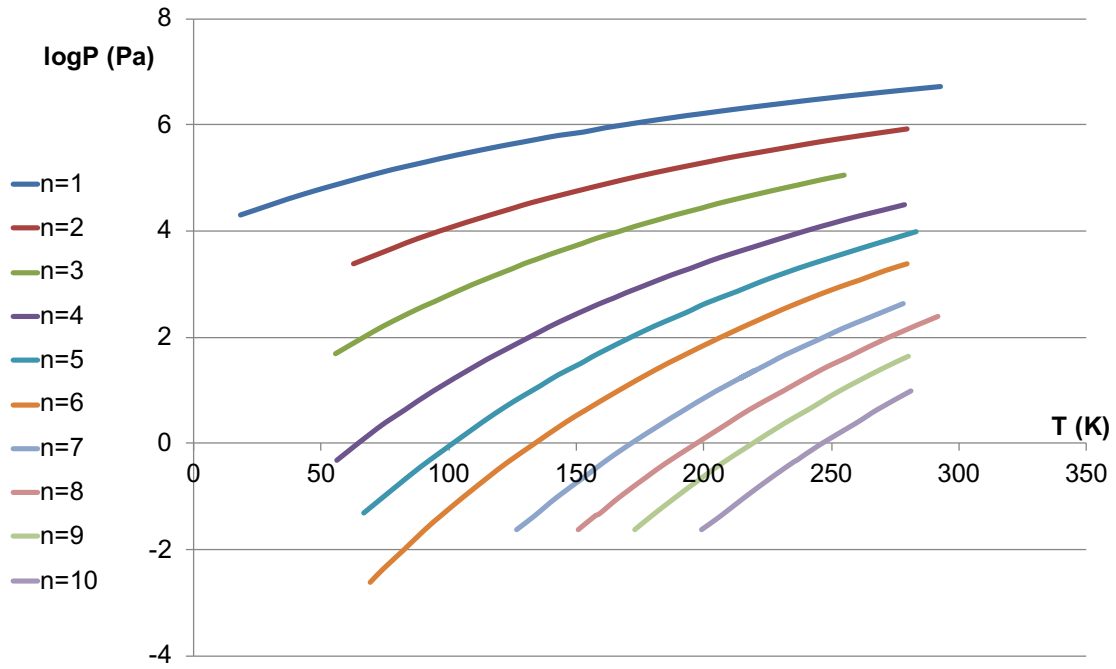


Figure 2.2: Plot of vapor pressure vs temperature for PEO oligomers with N values from 1 to 10.

The results for vapor pressures calculated from this model are not expected to be numerically correct, but they provide a good guidance in terms of the trend of vapor pressure curves and the gaps between neighboring N 's. For a specific N , vapor pressure increases with temperature; for a specific temperature, vapor pressure increases with N . X
More importantly, at a given temperature, the vapor pressures of two neighboring N 's have a difference up to two orders of magnitude. However, this difference is narrowed down as temperature goes higher, which indicates that it would be increasingly difficult to achieve a neat separation, and the isolation products are expected to be more polydisperse under higher evaporation temperature. Evaporation temperature should never get close

to 533K[11], which is the critical temperature where PEO starts thermal degradation in vacuum.

2.2 Evaporation technique and results

polydispersity as purchased?

Neat PEO sample was purchased from Sigma Aldrich, Inc., and it has an average M_n of 600, which appears as waxy solid at room temperature. The experimental setup for evaporative purification is generally the same as the setup used for polystyrene[?]. 96 mg of neat sample is placed on top of a polished silicon wafer of 2 cm \times 2 cm in size and 0.3 mm in thickness. Si wafer acts as a bottom substrate and is placed onto a Linkam hot stage in a home-built vacuum chamber. In order to collect isolated fractions, another Si wafer of 5 cm \times 5 cm in size is held approximately 3 mm right above the neat material, by thermal insulating spacers.

estra? Before the beginning of each evaporation period, the chamber is pumped down with a dry scroll pump to an initial pressure of around 0.3 mbar. After that, we flush the chamber with nitrogen, and then evacuate it again. This process is repeated for several times until there is little oxygen left in the chamber, to prevent the oxidation of polymer. Finally, we introduce a small amount of nitrogen into the chamber, until the pressure is raised to about 169 mbar. The reason for this action is because during the evaporation, the system requires a good thermal conduction to drive away excess heat from the hot stage, so to maintain a stable temperature (with a fluctuation of less than 1K) of the material.

We start the evaporation from 393K, and the evaporated material is collected every two

hours. Products from the first four hours are not collected, as they are expected to contain impurities such as initiators. We seal the product from each period into an aluminum sample pan, in preparation for future differential scanning calorimetry measurements and mass spectroscopy measurements.

Figure 2.3 shows that within each temperature region during the evaporation, the mass of material collected experiences a general decreasing trend, and the mass of products collected into sample pans ranges from 0.2 mg to 2.9 mg. We expected that each temperature region would correspond to a majority of a specific N, so different N's get isolated.

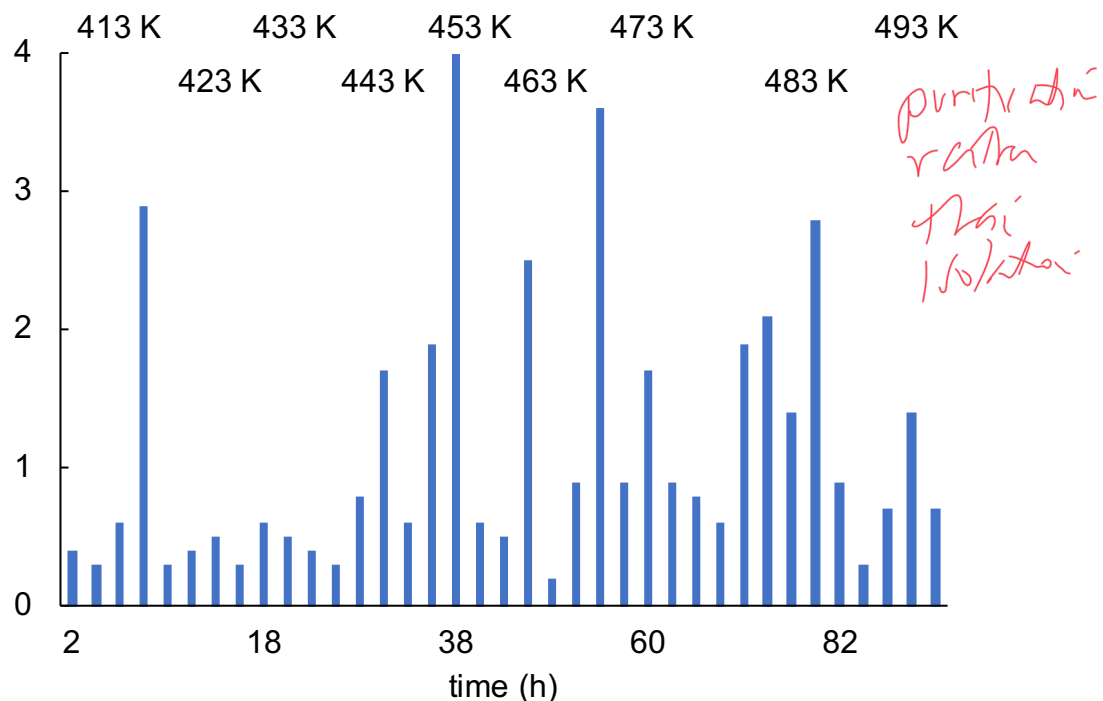


Figure 2.3: Mass of PEO collected with respect to time and temperature. (remember to label temperatures)

2.3 Results from mass spectroscopy

To obtain information about the actual distribution of different N's in each ~~isolated~~ fraction, mass spectroscopy measurements are performed on several samples. Matrix Assisted Laser Desorption/Ionization – time of flight (MALDI-TOF) technique was applied, with a Bruker Autoflex Speed MALDI-TOF mass spectrometer to conduct the measurements.

A typical MALDI-TOF mass spectroscopy works with the following procedure:

- Mix the analyte (polymer sample in our case) with appropriate matrix material.
- Bombard the mixed material with laser, and the laser energy is absorbed by the matrix, which get desorbed and ionized, and a phase transition from solid to gas takes place in the matrix material.
- A hot plume is generated, and during the flight of both the matrix material and the analyte, collisions among particles could result in the ionization of the analyte.
- Ions flying into the the TOF mass spectrometer are separated due to different mass (m)-to-charge (z) ratios. With the same kinetic energy, lighter ions arrive at the detector earlier than heavier ions.

From the spectrum generated, we ~~would~~ ^{are} be able to obtain information about the exact distribution of molecular weights, from which M_n , M_w , and PDI ~~could~~ be calculated.

can

2.3.1 MALDI-TOF spectra and analysis

MALDI measurements were carried out for 10 samples out of all the isolated fractions, the neat PEO sample, and the leftover sample after all the evaporation periods. Figure 2.4 compares the isolated fractions and shows the changes in molecular weight distribution during the evaporation process, with the green background spectrum being the neat sample.

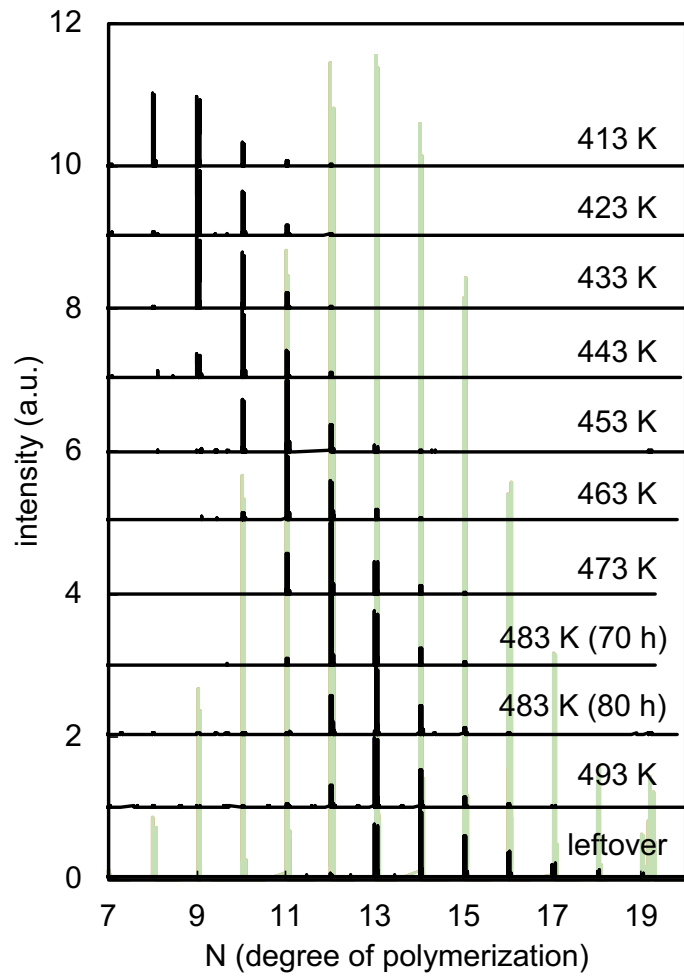


Figure 2.4: MALDI spectra of isolated products (black) and neat sample (green) (80 h: 80th hour since start of evaporation).

As the evaporation temperature increases, the N values composing of each isolated fractions shift towards higher values, ranging from 8 to 16. With the intensity of each peak, we are able to calculate their M_n , M_w , and PDI, and make quantitative comparisons. Compared to the neat sample, the spectra of isolated fractions are much narrower, meaning they are highly monodisperse. The lowest PDI we achieved is calculated to be 1.0052, which is around six times better compared to 1.0306 of the neat sample.

$(n-1)$

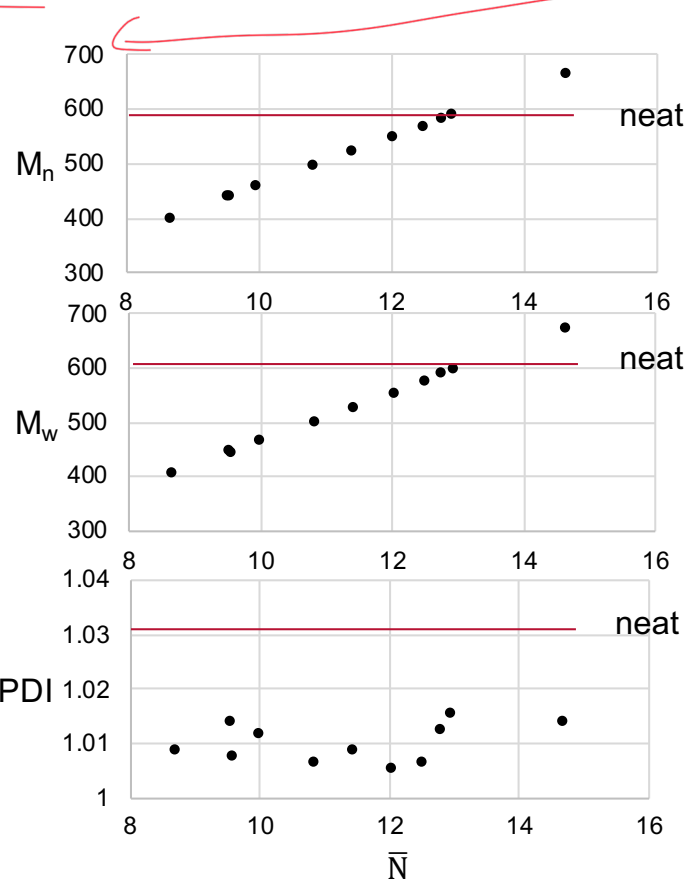
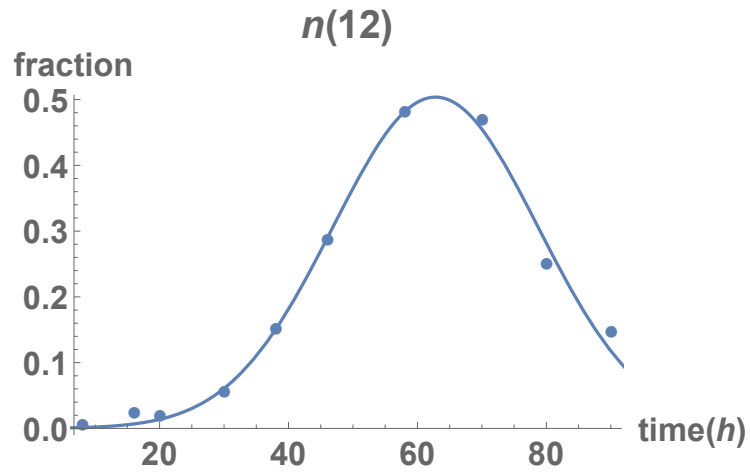


Figure 2.5: M_n , M_w , and PDI comparison between isolated fractions and neat sample.

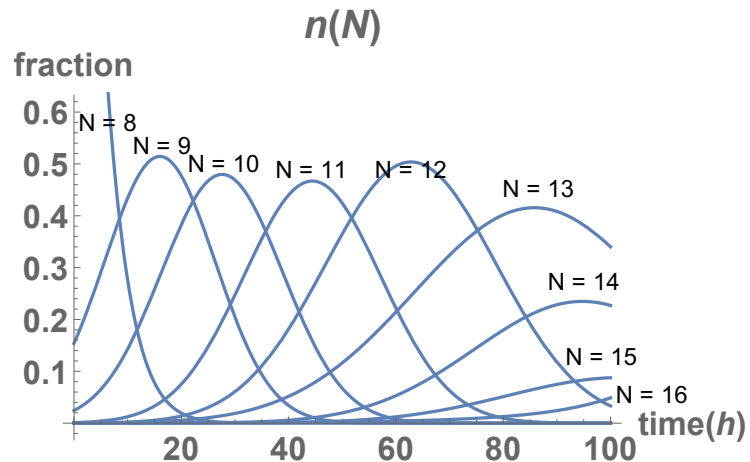
2.3.2 Evolution of N during evaporation process

So far ~~we have known~~ the distribution of N 's at these 10 points during evaporation. However, it would be ideal if we could generate the evolution of N values at any point without doing MALDI measurements on every single sample. In order to achieve this, we first plot the evolution of each N value with respect to evaporation time, based on the percentage fraction of each N in the isolated products from different points during the evaporation process. Then we fit the ten data points for each N value with Gaussian curves, which enables us to ~~get~~ the distribution of all N 's at any point during the evaporation (Figure 2.6). *estimath*

Interpolation!



(a) Percentage fraction of $N = 12$ in samples from different evaporation time.



(b) Evolution of N values (from 8 to 16).

Figure 2.6: Evolution of N values during evaporation process.

Chapter 3

not alone?

Crystal structure analysis

3.1 Polymer crystallization

3.1.1 Polymer crystal models and theories

Upon cooling, materials transform into a lower energy state. A regular liquid under such conditions transition into amorphous state or crystalline state (the ground state). For a polymer, the chains are entangled and aligned in all directions in liquid state, so it is much more difficult to achieve its ground state, with the monomers sitting on crystal lattice points and the chains aligned perfectly parallel with each other. However, polymers could still crystallize under proper conditions, adopting a more complex structure rather than the ideal crystalline state, and this process does not only depend on thermodynamics, but kinetics as well.

Before we look at long polymers chains, oligomers (especially linear ones) are a simpler

yet close enough example in terms of crystallization. Based on X-ray crystallography results, oligomer crystals adopt a structure of stacked layers, with each layer composed of chains standing up perpendicular to the layer surface (Figure 3.1). Among neighboring layers, end-groups of the chains form the amorphous phase at the interfaces.[1]

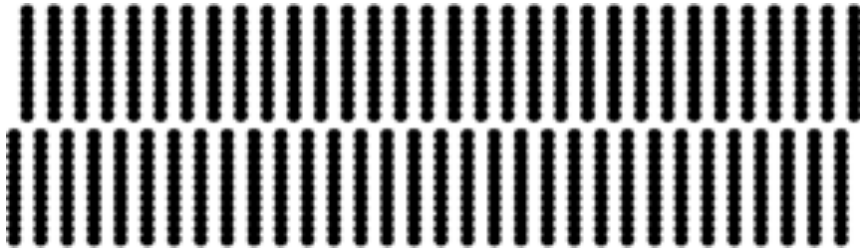


Figure 3.1: Oligomer crystal structure. [1]

For crystallization of polymers with higher molecular weights, however, it is impossible for the chains to completely disentangle, which requires an extremely high energy and a very long time. Limited by the nature of polymers themselves, the chains align into local crystalline domains, with some unresolved entanglements left as amorphous phases in between. End-groups are also part of the amorphous phase. Therefore, polymer crystals are called semicrystalline crystals.

(Inconsistent with your firs¹ one.)

Fringed micelle model

In order to describe semicrystalline polymer crystal structures in further details, different models and theories have been proposed. One of the earliest models is fringed micelle model [12]. In this model, both the crystalline phase and the amorphous phase are present, with

the crystallites existing as local domains. The micelles of crystalline parts have sizes much smaller than the chain lengths, so a single polymer chain is believed to be able to pass through several micelles, thus binding them together.

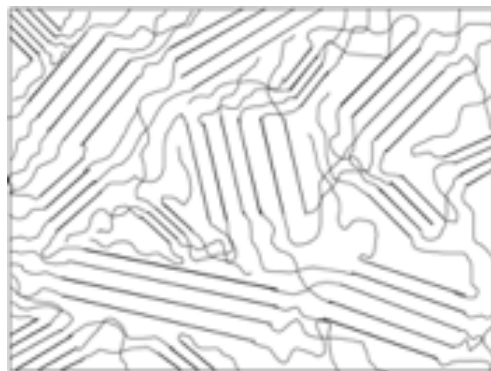


Figure 3.2: Fringed micelle model of polymer crystal structure. [2]

Before long, problems started to rise for fringed micelle model. According to the calculation of free energy, it was found that there would be a large conformational entropy loss for the amorphous chains if this model was true [13]. In addition, experimentalists observed evidences of large crystallites - “sperulites”, which have a strong preference in terms of the alignment of chains, and are highly symmetrical instead of a random distribution of crystallites [14]. Together with some other flaws and contradictions found with the model itself [15, 16], people began to doubt this model and try to find other ways to describe semicrystalline polymer crystals.

↓
unclear what you
are referring to

Folded chain model

*Content
is for
10/8*

As the fringed micelle model was being questioned, some crucial experimental observations led to the birth of a new model of polymer crystals—the folded chain model. The concept of chain-folding was actually first proposed by Storks, when he observed unstretched films of gutta-percha through electron diffraction measurements and found that the films are composed of large crystallites with the chain axis perpendicular to the film surfaces. The thickness of the films are much smaller than the chain lengths, which led to Storks' proposal that the chains need to fold themselves inside the film [17]. At that time, fringed micelle model was still dominating the directions of polymer crystallization researches, so his results and proposal did not receive much attention. Later, several researchers [18, 19, 20] studied polymer single crystals and found that they have smooth surfaces, with heights of about 10 nm, which is also much smaller than the chain lengths. The chains are believed to fold themselves back and forth in each lamella, and when the polymer solution concentration is high enough, or when the polymer crystallizes from a melt, multiple lamellae stack together to form a crystal. These observations helped the development of folded chain model, which from then on became the most widely accepted model of polymer crystals.

Now it is clear that the chains fold in crystal, and next step would be to determine the way of chain folding. After the chain gets to the amorphous interface and fold itself back, it is not clear where it re-enters the lamella. There have been a large number of studies on this [7, 21, 22] and two major models have been proposed: adjacent re-entry model and random re-entry model.

As adjacent re-entry model describes, after a chain escapes the lamella and makes a

fold, it immediately returns and inserts back into the neighboring site. In this way, the lamellae created have relatively smooth surfaces, as Figure 3.3 shows.

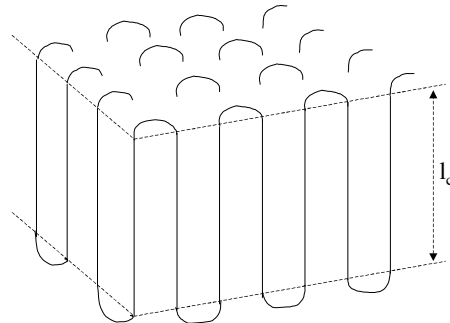


Figure 3.3: Adjacent re-entry model of polymer crystals [3].

Random re-entry model is also known as switchboard model. Instead of folding right back into the neighboring site on the same lamella, a chain that emanated from the lamellar surface could either float on the interface and walk into a further site, or even enters a neighboring lamella, which leads to a completely random arrangement on the interfaces of lamellae and amorphous regions (Figure 3.4).

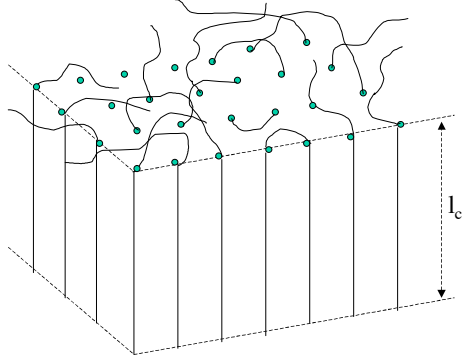


Figure 3.4: Random re-entry model of polymer crystals [3].

Adjacent re-entry model would result in a much more thermodynamically favorable conformation with a lower entropy. However, in a real situation of polymer crystallization, twisting, misalignment, and entanglements of the long chains prevent them from relaxing and aligning perfectly in regular folds. Instead, regions consisting too many entanglements are more likely to be shifted to the surfaces and contribute to the amorphous phase [1]. Taking both thermodynamics and kinetics factors into account, real polymer crystal lamellae are normally composed of both adjacent re-entries and random re-entries. It should be noted that in real cases, chain-folding also depends on more factors: chain lengths, flexibility of chains, crystallization temperature, cooling rate, chain defects, etc.

3.1.2 Thermodynamics of polymer crystallization

Thermodynamics is the fundamental rule that polymer chains obey during crystallization. The most favorable state for polymers is that with the lowest possible free energy G . G is

lower for melt than for crystals at high temperatures, while it is lower for crystals than for melt at low temperatures. The equilibrium melting point T_m^∞ is defined as the temperature at which the liquid state and the solid state have the same free energy. Therefore, the change in Gibbs free energy, ΔG , is equal to zero during melting or crystallization transition at thermodynamic equilibrium:

$$\Delta G = \Delta H - T_m^\infty \Delta S = 0 \quad (3.1)$$

$$T_m^\infty = \frac{\Delta H}{\Delta S} \quad (3.2)$$

In practical cases, the crystallization temperature T_c is always lower than the melting temperature T_m , and their difference is defined as the supercooling ΔT . This is mainly due to the nucleation and growth mechanism during crystallization. A nucleus must be present to initialize the growth of a crystal, and when there is no present nuclei, the temperature needs to keep decreasing until the melt itself starts a primary nucleation. This mechanism will also be further discussed in Chapter 4. Compared to regular crystals, ΔT of polymers could be as large as 20 to 30 K, resulting from the metastable chain-folding nature of polymers [23].

Equation 3.2 tells us that the equilibrium melting temperature depends on both enthalpy and entropy of the system. However, the effect of surface energy and crystal size has not been considered. For a real polymer crystal, shape and size of the lamella would directly affect its melting point, and this effect could be examined through thermodynamics.

Let us start with an infinitely large crystal, and from conventional thermodynamic viewpoints it is considered not to involve surface energy. Therefore its melting point is believed to be T_m^∞ .

Now assume a lamella with length a , width b , and height l , where $a \gg l$, and $b \gg l$. The surface energy per unit area of the top and bottom surfaces is σ_e , and the surface energy per unit area of the side surfaces is σ . This lamella with the finite size effect could be considered as a quasi-two dimensional object with one-dimensional confinement [24]. The free energy per unit mass on melting is Δg , and the total free energy ΔG on melting consists of the energy required to create new surfaces and the energy of fusion for the bulk:

$$\Delta G = 2(a + b)l\sigma + 2ab\sigma_e - abl\Delta g \quad (3.3)$$

and with $\sigma_e \gg \sigma$, $a \gg l$, $b \gg l$, the total free energy is then:

$$\Delta G = 2ab\sigma_e - abl\Delta g \quad (3.4)$$

At melting temperature T_m , $\Delta G = 0$, which leads to:

$$\Delta g(T_m) = \frac{2\sigma_e}{l} \quad (3.5)$$

Once again, for an infinitely large crystal, we have:

$$\Delta g(T_m^\infty) = \Delta h(T_m^\infty) - T_m^\infty \Delta s(T_m^\infty) = 0 \quad (3.6)$$

Assuming between T_m and T_m^∞ , the enthalpy and entropy do not have a significant change, we further have:

awkward wording

$$\Delta g(T_m) = \Delta h(T_m) - T_m \Delta s(T_m) \quad (3.7)$$

Combining Equation 3.6 and Equation 3.7, we are able to generate:

$$\Delta g(T_m) = \Delta h(T_m) - T_m \frac{\Delta h(T_m)}{T_m^\infty} \quad (3.8)$$

Now with Equation 3.5 and Equation 3.8, we finally obtain the relation between the thickness of a lamella and its melting temperature:

$$T_m = T_m^\infty \left(1 - \frac{2\sigma_e}{l\Delta h}\right) \quad (3.9)$$

which is the well-known Gibbs Thomson equation. It has been applied to many polymers with linear structure and has proved to provide reliable predictions of the melting temperature as a function of lamella thickness [25]. With a larger thickness, the finite size effect is weaker, and the melting temperature T_m of the lamella would be closer to the equilibrium melting temperature T_m^∞ .

might say a little why PEO
is an important polymer
unless in CHI

3.2 PEO crystallization

In terms of crystallization, PEO is one of the most intensively studied polymers, together with Poly(Ethylene) and n-alkanes. With a linear structure, these polymers all crystallize very easily. As a semicrystalline polymer, PEO chains fold into lamellar structures during crystallization process, and multiple lamellae stack up to form the whole crystal [26]. In our case, we focus on low molecular weight PEO, so crystallization should be even easier since the chains are relatively short and thus need fewer times of folding. When the number of folds changes, the thickness of the lamella varies, which has a direct influence on the melting temperature of the crystal lamella.

3.2.1 Crystal structure

PEO crystals have monoclinic unit cells, with the chains adopting a structure of 7/2 helix with trans-gauche-trans conformation. In this conformation, seven monomeric units form two periods of the helix, which is 1.93 nm long [4]. As shown in Figure 3.5, every bond is rotated by a certain angle with respect to the c-axis (vertical axis) of the lamella, and the projection length of one monomer on the c-axis, l_c , is 0.278 nm [27].

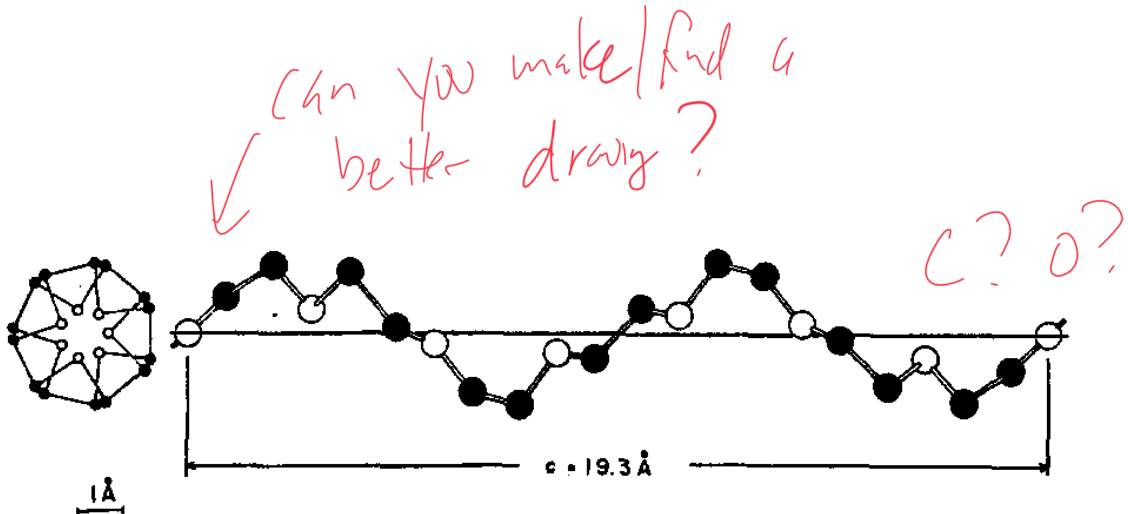


Figure 3.5: A skeletal model of PEO molecule in the crystalline state [4].

Low molecular weight PEO fractions, or PEO oligomers, crystallize with chains folded a small number of times, or even fully extended [7, 28]. The number of folds depends on many factors including crystallization temperature, chain length, cooling rate, etc. The thickness of the lamella L is thus determined by the number of folds n and the chain length λ :

$$L = \frac{\lambda}{1+n} = \frac{Nl_c}{1+n} \quad (3.10)$$

where N is the number of monomers in a chain, or the degree of polymerization. Especially for fully extended chains, $n = 0$, and the thickness of the lamella is equal to the chain length.

In terms of chain folding, we have also discussed about the two different chain re-entry models in 3.1.1: adjacent re-entry model and random re-entry model. In the case of PEO oligomers, the chains are relatively short, and there are not as many entanglements among the chains, so we could expect more adjacent re-entries in the lamellae.

3.2.2 Melting points of PEO oligomers

Gibbs Thomson equation (Equation 3.11), enables one to build the relation between melting points and other physical parameters of a polymer crystal. In order to be consistent with other researches on PEO melting transitions, here we make some modifications to the original equation:

$$T_m = T_m^\infty \left(1 - \frac{2SV}{L\Delta H}\right) \quad (3.11)$$

where S is the surface free energy of the interface between the crystalline and the amorphous phase, and V is the molar volume of a crystallizable repeat unit [29]. In this equation, T_m^∞ , V , and ΔH are constants that have been determined for PEO.

Melting transitions of PEO have been intensively studied through various experimental methods and from different theoretical aspects. Among the large number of researches, there is a fundamental one that is particularly of our interest and worth being reviewed. Relatively monodisperse PEO oligomers with the degree of polymerization ranging from 9 to 45 were produced through step-wise syntheses by Yeates et al [5]. Melting points of these fractions were measured, and compared to those of commercially available samples, which are much more polydisperse. Their results are shown in Figure 3.6.

awkward writing!

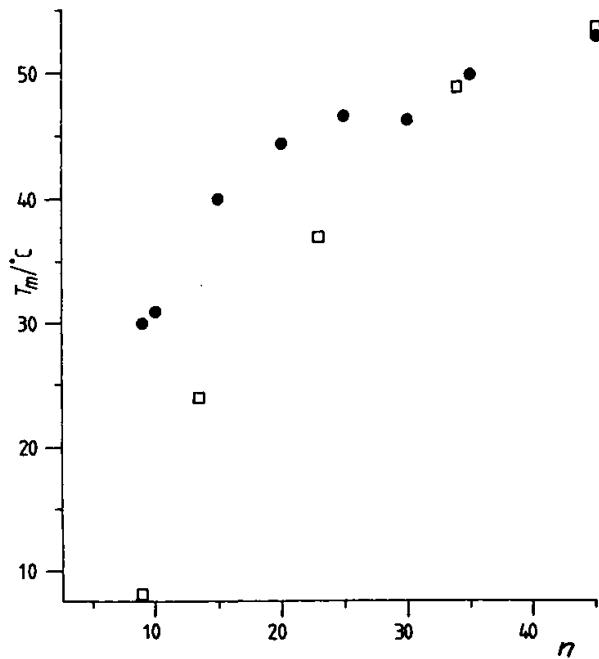


Figure 3.6: Melting points vs degree of polymerization for monodisperse (black dots) and polydisperse (empty boxes) PEO oligomer samples [5].

Melting points of monodisperse samples are notably higher than those of polydisperse samples in general, and the difference is especially large for small N values. This observation indicates that polydispersity has a big influence on melting temperature, and in fact became one the motivations that we conducted crystallization experiments with our isolated products, so that we could further investigate this phenomenon.

As a matter of fact, this observation has attracted much attention from researchers.

People have proposed different explanations and one of them suggests that the T_m difference could be related to the chain end-groups [30]. In a relatively monodisperse sample, chains

have roughly the same length, which makes it easier to create a smooth lamellar surface, and the end-groups would be incorporated in the crystalline array. However, in a polydisperse sample, the distribution of chains results in a more disordered lamellar surface, so some of the end-groups have to be incorporated in the amorphous phase. Because of the difference in the incorporation of chains ends, polydisperse crystals would have lower crystallinity and higher entropy, which leads to a higher melting temperature.

3.3 Basics of differential scanning calorimetry

The isolated products pressed into Al pans previously are characterized with a differential scanning calorimeter (DSC) (Q100, TA Instruments). DSC is an instrument that measures the heat capacity change of the sample material within a controlled temperature range. Inside a typical DSC there are two metal (Al commonly) pans, with one acting as the sample pan and another empty pan acting as a reference. Through precise heating and cooling control with a feedback mechanism, the two pans are maintained at the same temperature at any time during the scanning measurement. At temperatures where phase transitions of the sample material takes place, the heat capacity of the sample changes, which requires the computer to adjust the amount of heat flow provided, in order to always keep the two pans at the same temperature. The heat flow $\frac{dQ}{dt}$ could be obtained as a function of temperature, which depends both on the heat capacity C_p of the sample and the scanning rate q :

$$\frac{dQ}{dt} = \frac{dQ}{dT} \cdot \frac{dT}{dt} = C_p q \quad (3.12)$$

might be worn having a short
 "phase transition in polymer" section
 melting $T_g \rightarrow$ No Latent heat \Rightarrow Kinetic tran
 $T_m \rightarrow$ Latent heat \Rightarrow Thermodynamic tran.

By plotting the difference in heat flow to the two pans with respect to temperature, thermal transitions the sample material experienced during the set range of temperature, such as crystallization, melting, and glass transition, could be determined. Figure 3.7 is a typical DSC curve. When the scanning rate is constant, first-order transitions appear as peaks on the DSC curve. Crystallization appears as an exothermic peak on the cooling curve, and melting appears as an endothermic peak on the heating curve. The difference observed between the crystallization temperature T_c and the melting temperature T_m is supercooling ΔT . Note that here in this figure crystallization and melting are presented on the same curve for the sake of neatness, but they in fact occur on separate curves.

$C_p?$

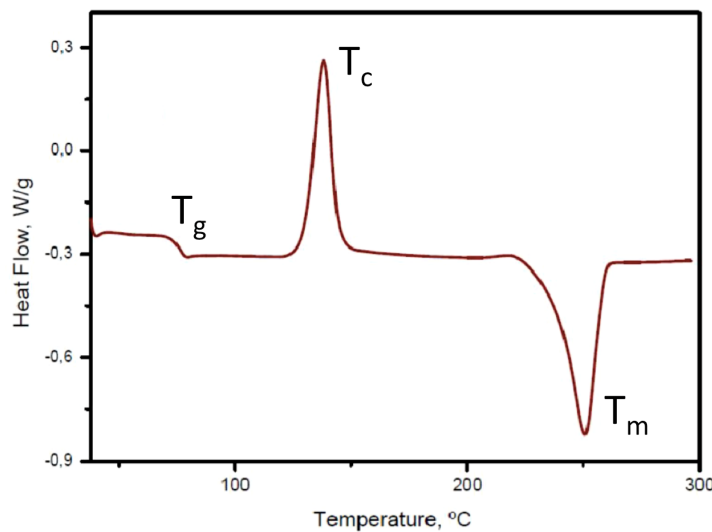


Figure 3.7: A typical DSC curve for a polymer sample [6].

3.4 Results from differential scanning calorimetry

The following running process is performed on each isolated product: equilibrate at 353 K; isothermal for 5 min; ramp 10 K/min to 173 K; isothermal for 5 min; ramp 10 K/min to 353 K; isothermal for 5 min; ramp 10 K/min to 173 K; isothermal for 5 min; ramp 10 K/min to 353 K.

Uhy?

3.4.1 Melting temperature

From the DSC curves of each fraction, we determined their melting temperature, T_m , as shown in Figure 3.8. Most of the samples show a double-peak pattern, with a lower T_{m1} and a higher T_{m2} . Each measurement is carried out for more than once, and the T_m values from separate measurements normally vary within ± 2 degrees. \bar{N} is the average N value of each sample, which is interpolated linearly based on the 10 samples measured with MALDI. In general, the melting temperatures behave as Gibbs Thomson relation describes, with the higher N values (longer chains) showing higher melting temperatures.

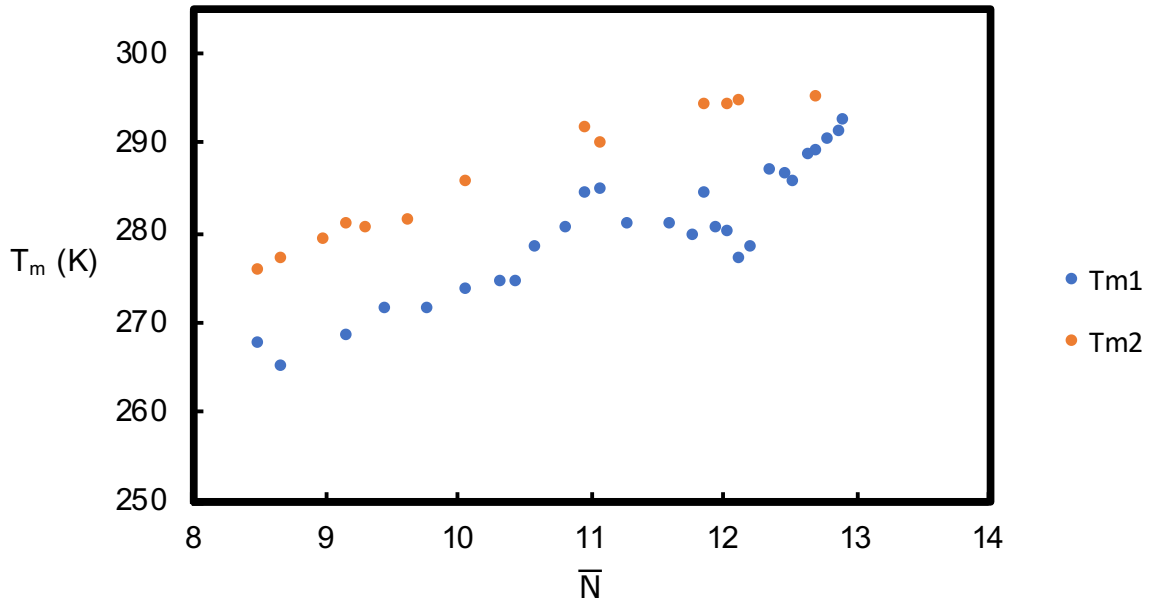


Figure 3.8: Melting temperature of isolated fractions.

Chain-folding analysis based on T_m

In figure 3.8, it is obviously seen that the data points potentially lie on two parallel curves, which brings our assumption that they could correspond to two types of chain-folding modes in the crystal lamellae, with the higher T_m 's being extended chains (larger thickness), and the lower T_m 's being once-folded chains (smaller thickness).

In order to validate our assumption, we apply Equation 3.11 to see if we are able to get a good fit with the two series of data. Parameters for PEO present in this equation, including T_m^∞ [31], V [32], ΔH [33] are found in the literature. Interfacial tension S is dependent on the mode of chain-folding, as both chain ends and chain folds contribute to

the amorphous phase, and they lead to different interfacial tensions with respect to the crystalline phase.

Interfacial tension of chain folds, S_{folds} , could be obtained from parameters of PEO chains with large enough molecular weights. This is because in the crystal lamellae of long chains, the number of chain folds are much greater than that of chain ends, and thus S is dominated by chain folds. For long PEO chains, crystal lamellar thickness L is normally on the order of 10 nm [34], and the melting temperature of high molecular weight PEO is around 65°C [35]. With the other parameters previously found, we are able to calculate S_{folds} from Equation 3.11.

However, to quantitatively look at the thermodynamics of extended chains and once-folded chains in our assumption, and to fit Gibbs Thomson relation of these two modes to our data, we are required to know the actual interfacial tensions in these two modes. For ~~extended chains~~, the interfacial tension merely comes from chain ends, and for once-folded chains, both chain ends and chain folds contribute to the interfacial tension. S_{ext} and S_{1-fold} could be obtained by adjusting their values based on S_{folds} , because they should be on the same scale. For extended chains, we fit the higher melting points with Gibbs Thomson equation, using the value of S_{folds} initially, and then adjust its value until we get a good enough fit (Figure 3.9). This value is then taken as S_{ext} .

Under ~~that~~ conditions
make any prediction!

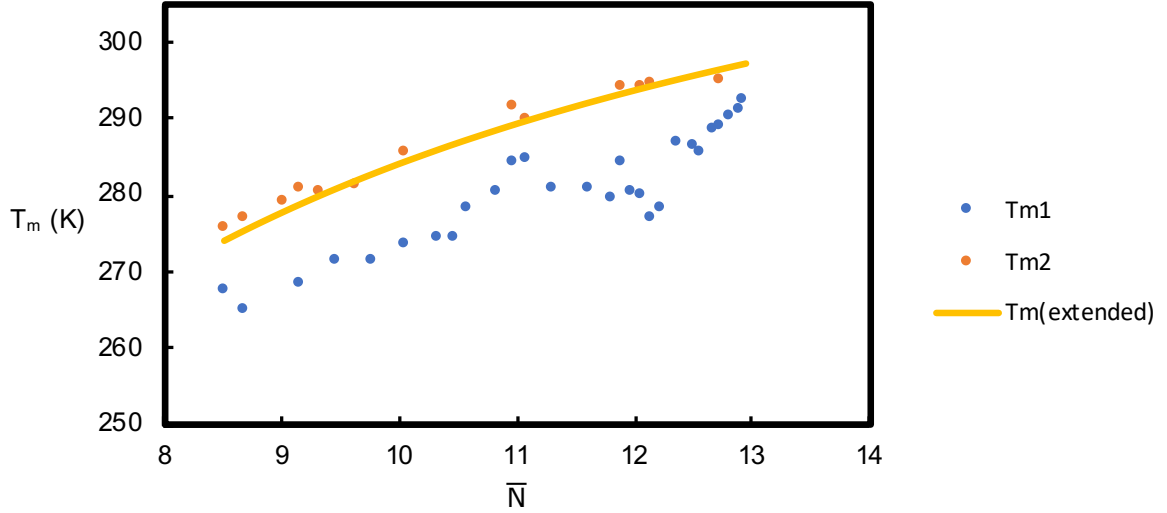


Figure 3.9: T_{m1} data fitting to Gibbs Thomson equation.

For the lower melting points, which correspond to once-folded chains, the chains emanating from the lamella enter the amorphous phase to make a fold, and then re-enter the lamella. In this case we suppose that it takes N_a monomers for a single chain to complete this turn, instead of bending 180° sharply. This conformation has two chain-end monomers on one side of the lamella, and N_a monomers on the fold on the other side, which enables us to calculate the interfacial tension S_{1-fold} as:

$$S_{1-fold} = \frac{2S_{ext} + N_a S_{folds}}{2 + N_a} \quad (3.13)$$

With S_{1-fold} obtained, the value of N_a is now the only free parameter that could be tuned to fit the lower melting points with Gibbs Thomson equation. From the curve fitting

(Figure 3.10), N_a is determined to have a value of 3.5. For a PEO chain, this is approximately 2.6 times its persistence length [27], which suggests that this chain conformation is a possible and reasonable model of chain-folding.

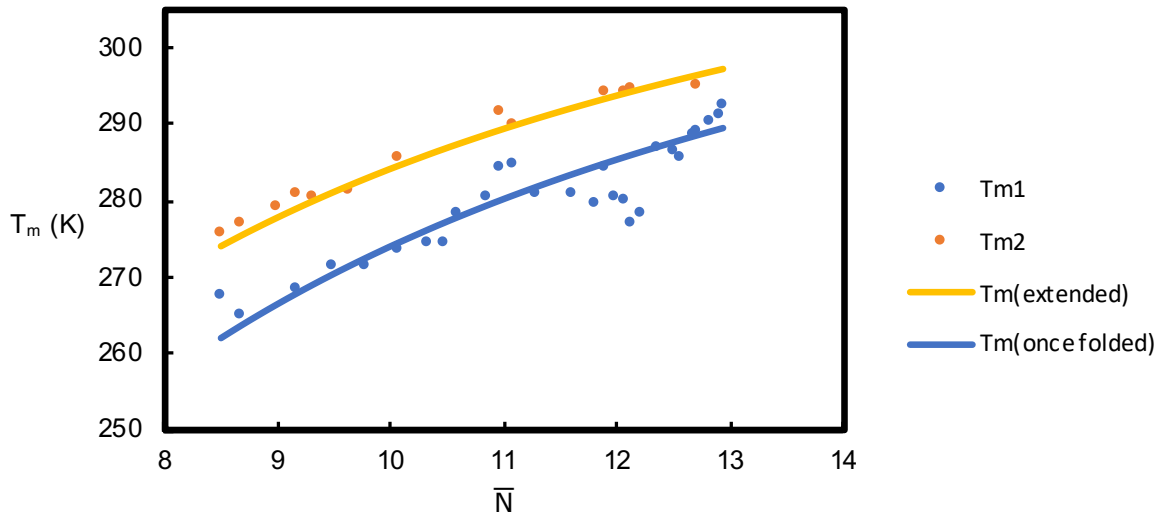


Figure 3.10: T_{m1} and T_{m2} data fitting to Gibbs Thomson equation.

In the plots of melting temperatures, the x-axis, \bar{N} , is the number average value of all the composing N 's in each isolated fraction, characterized directly with MALDI or interpolated based on the MALDI data. However, only with single integer N values could we be able to talk about the melting temperatures given by the Gibbs Thomson curves. For a mixtures of different N 's, its melting temperature potentially lies anywhere within the range of T_m 's of its composing N 's. A more careful way to present our chain-folding models together with the T_m data would be as Figure 3.11 shows. A vertical bar is generated for

each T_m point, with the top of the bar representing the melting point of the highest N value present in this fraction, and the bottom of the bar representing the lowest N value in the fraction. In generating the bars, N components with a percentage less than 5 % are neglected. Notice that the two curves cross most of the bars,

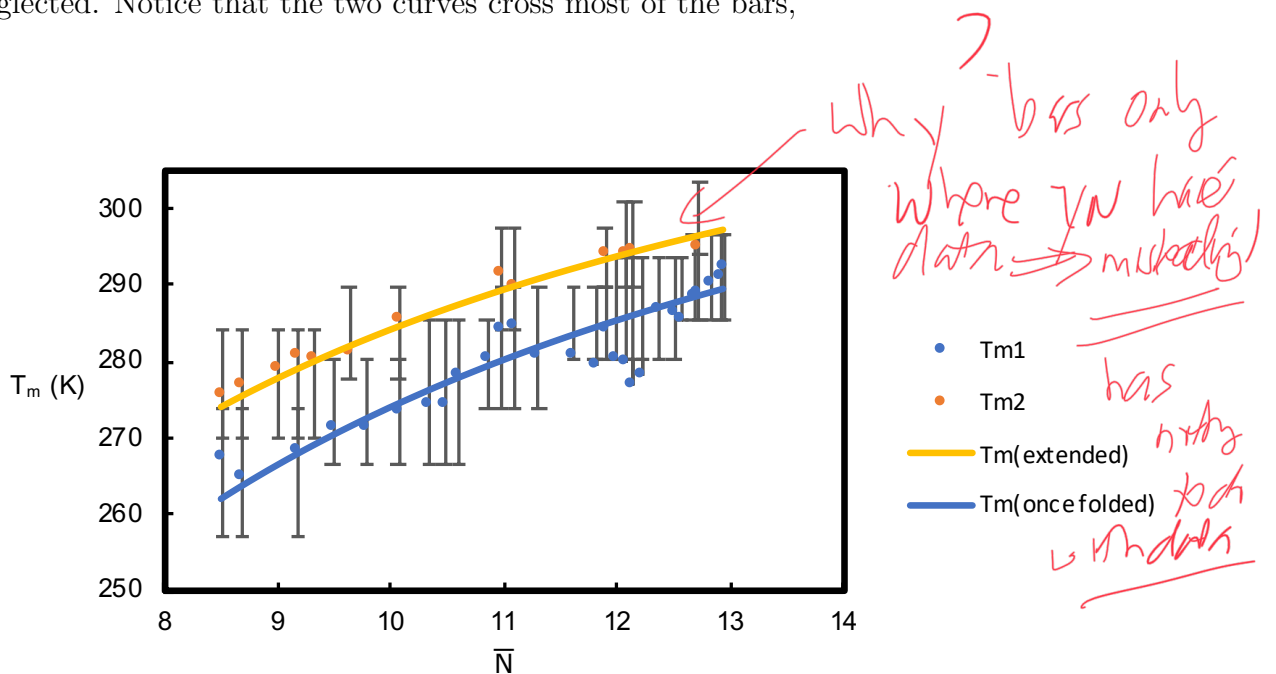


Figure 3.11: Gibbs Thomson relation fitting with potential range bars on T_m data points.

In the DSC measurements, fractionation of chains with different N 's is sometimes observed. During some of the repeated DSC measurements, several isolated samples show double melting peaks, with both near the same T_m curve. The two peaks are separated by around 3 K, which is likely the difference between the melting temperatures of two neighboring N 's according to our calculation, rather than the difference between the two chain conformations (extended and folded). It is worth noting that this fractionation is

more commonly observed at the higher T_m than at the lower T_m , because in the extended conformation, the crystal lamellae composing of two neighboring N's have a large difference in thickness than in the folded conformation.

Tuning chain-folding mode

Most of the fractions show two melting points in DSC measurements, while some of the fractions only shows one, either lying on the T_{m1} curve or the T_{m2} curve. For these fractions, when the lower T_m is observed, on the cooling ramp during DSC measurements there is only one crystallization peak, which is an indication that the cooling rate during crystallization process may not have been slow enough for the chains to crystallize in the extended form. However, when the higher T_m is observed, on the cooling ramp there are usually two crystallization peaks, suggesting that the polymers still form both extended chains structure and folded chains structure, but before increasing to the melting temperature, once-folded chains relax themselves and recrystallize into extended form.



The following treatment (Figure 3.12) is then applied to further verify our observation. With some of the fractions that show the lower T_m (either with or without the higher T_m) in normal DSC measurements, we keep the sample at a temperature between T_{m1} and T_{m2} for a time long enough to melt all the once-folded chains and leave all the extended chains. Then we cool the sample to a much lower temperature, and measure its melting again. During the second DSC measurement only the higher T_m appears, which is a direct proof that we have successfully forced the once-folded chains to recrystallize into extended chains by applying the treatment.

*before and after
DSC?*

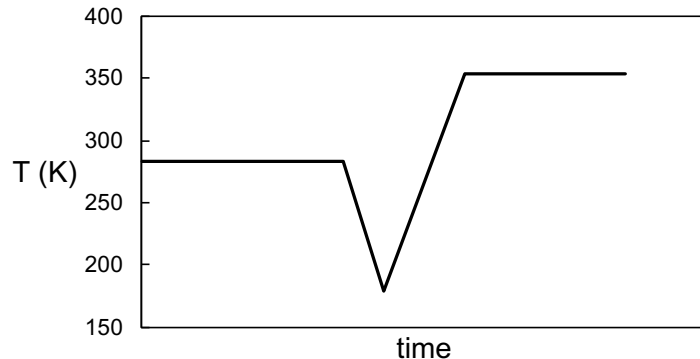


Figure 3.12: Thermal treatment on some of the isolated fractions.

Comparison between isolated fractions and neat sample

When we compared the DSC curves of the neat sample and the isolated fractions, surprisingly we noticed that some of the fractions performed unexpected melting behaviors, as Figure 3.13 shows. From the curves of some products from early stages of evaporation, we expect that in the neat mixed sample they should start melting at temperatures much lower than the observed melting temperature of the neat sample. However, this is not what happens. According to this phenomenon, we believe that when the short chains are mixed with longer chains, they become influenced and perform different crystallization behaviors than in a more monodisperse sample. One of the possible explanations to this is that in the presence of longer chains, the shorter chains tend to act as amorphous phase, even at temperatures lower than the melting points of themselves. As a matter of fact, it is also possible that the short chains only take up a very small portion in the neat sample, therefore the heat flow signal from them could easily be overwhelmed by that of major

components.

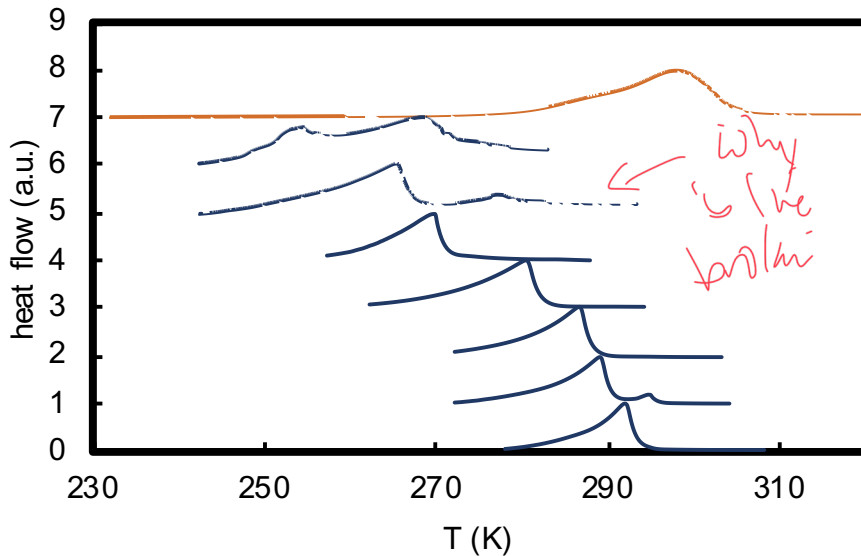


Figure 3.13: DSC curves of the neat sample and some of the isolated fractions.

End-group effects

In 3.2.2, we reviewed Yeates' study on melting of monodisperse and polydisperse PEO oligomers. Now we would like to bring our results for isolated fractions into comparison with theirs. Surprisingly, it turns out that the melting temperatures we obtained agree more with the polydisperse samples in their measurements. This could be an indication that the melting points difference they observed between the monodisperse and polydisperse samples is very unlikely to be due to polydispersity. Instead, it could be related to specific properties such as end-group chemistry.

End-group effects on PEO crystallization has been studied by many researchers and it

SOUND) WEAK

has been found that the type of end-groups directly influences properties including melting temperature and crystallinity. Monodisperse PEO with hydroxy end-groups has been reported [36] to display different crystallinity and T_m 's than that with methoxy end-groups. The difference in crystallinity was believed to be due to different heats of interaction related to the end-groups at the lamellar surfaces. The difference in melting temperature was attributed to different environments at a crystalline lamellar surface and in melt, because lamellar surfaces are much more ordered compared to the melt, which magnifies the effect of end-groups on the surfaces. Polydisperse PEO samples with different end-groups, however, display different crystallinities but similar T_m 's. Rejection of methoxy end-groups from the lamellar surfaces results in higher entropy of the crystal, leading to a lower enthalpy of melting, and a lower crystallinity. In terms of the melting temperature, it is claimed that the disordered lamellar surface and the melt have similar environments, so the effect of end-groups on T_m 's would appear less significant.

In our experiments, the PEO samples only contain hydroxy end-groups, while in Yeates' study, the synthesis of monodisperse samples involved end-groups containing sulfur. Based on the evidences and analysis mentioned above, sulfur could have resulted in different interaction energy with the crystalline layer, and potentially led to different melting temperatures. *How would S change interfacial energy?*

3.4.2 Degree of crystallinity

PEO has been known as a polymer with high crystallinity due to its linear structure. However, based on the fact that polymers almost never crystallizes completely, it is of interest

to study the degree of crystallinity X_c of our samples. We determine X_c of the isolated products from the heat of fusion $\Delta H_f(T_m)$ on melting in DSC measurements. The heat of fusion could be calculated from the area under the melting peak, and the degree of crystallinity is defined as [37]:

$$X_c = \frac{\Delta H_f(T_m)}{\Delta H_f^0(T_m^0)} \quad (3.14)$$

where X_c is the degree of crystallinity by weight fraction, $\Delta H_f(T_m)$ is the enthalpy of melting transition, and $\Delta H_f^0(T_m^0)$ is the enthalpy of melting of PEO with 100 % crystallinity [33]. By integrating the melting peaks on the DSC curves, we obtain X_c of the isolated products, as shown in Figure 3.14.

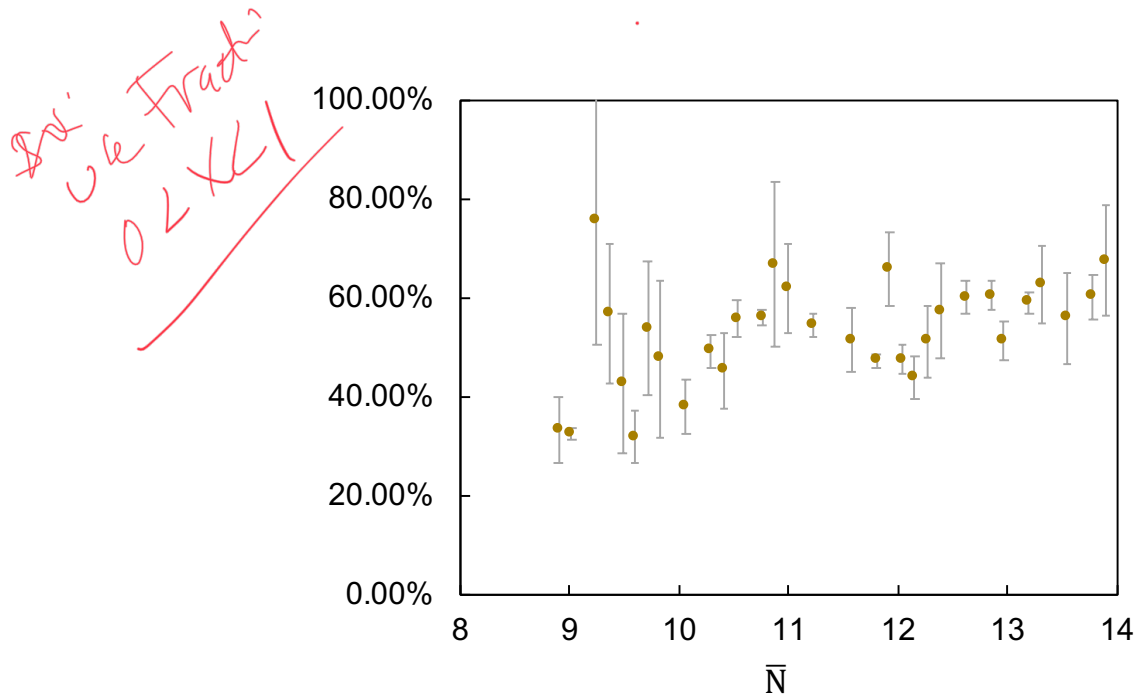


Figure 3.14: Degree of crystallinity of isolated products.

Compare b other studies?

It is easily noticed from the figure that our data is not precise enough since the error bars for some of the fractions are quite large. This results from the deviation (0.1 mg) of the scale used to weigh the samples. The enthalpy of melting $\Delta H_f(T_m)$ calculated from the DSC curve is directly related to the weight of sample, and for samples with a small weight, the deviation is comparable to its weight. Therefore, for more precise data of X_c , larger amount of sample is required, which brings forward the demand for technical improvements including scaling-up of our evaporative purification system.

An interesting fact about the X_c data is that when we bring Figure 3.14 and Figure 3.8 into comparison (even though X_c and T_m are not directly related), it could be noticed

no figure?

that they have a similar trend, especially with the bump pattern located at \bar{N} around 11. However, the reason behind this observation is still unclear to us and needs further investigation.

References

- [1] Gert Strobl. *The physics of polymers: Concepts for understanding their structures and behavior.* 2007.
- [2] Paul J. Flory. *Principles of polymer chemistry.* Cornell University Press, 1953.
- [3] Advanced High and Strength Steels. Chapter 2 . Literature Review. pages 7–78.
- [4] Toshio Yoshihara, Hiroyuki Tadokoro, and Shunsuke Murahashi. Normal vibrations of the polymer molecules of helical conformation. IV. Polyethylene oxide and polyethylene-d4oxide. *The Journal of Chemical Physics*, 41(9):2902–2911, 1964.
- [5] Stephen G. Yeates, Hoon Hong Teo, Richard H. Mobbs, and Colin Booth. Ethylene glycol oligomers. *Makromolekulare Chemie*, 185(8):1559–1563, aug 1984.
- [6] Marcelo Y Misutsu, Leandro F Cavalheiro, Thiago G Ricci, Luiz H Viana, Silvio C De Oliveira, Amilcar Machulek Junior, and Lincoln C S De Oliveira. Thermoanalytical Methods in Verifying the Quality of Biodiesel. *Biofuels - Status and Perspective*, 2015.
- [7] A J Kovacs, C Straupe, and A Gonthier. Isothermal growth, thickening, and melting of polyethylene oxide) single crystals in the bulk. II. *Journal of Polymer Science: Polymer Symposia*, 59(1):31–54, 1975.
- [8] S. Zhu, Y. Chai, and J. A. Forrest. Evaporative purification to produce highly monodisperse polymers: Application to polystyrene for $n = 3 – 13$ and quantification of T_g from oligomer to polymer. *Physical Review Materials*, 1(2):025605, jul 2017.
- [9] Isaac C. Sanchez and Robert H. Lacombe. An elementary molecular theory of classical fluids. Pure fluids. *Journal of Physical Chemistry*, 80(21):2352–2362, 1976.

- [10] P A Rodgers. Pressure Volume Temperature Relationships for Polymeric Liquids: a Review of Equation of State and their Characteristic Parameters for 56 Polymers. *J. Appl. Polymer Sci.*, 48:1061–1080, 1993.
- [11] Andrei Choukourov, Andrey Grinevich, Oleksandr Polonskyi, Jan Hanus, Jaroslav Kousal, Danka Slavinska, and Hynek Biederman. Vacuum Thermal Degradation of Poly (ethylene oxide). *J. Phys. Chem. B*, 113(Figure 1):2984–2989, 2009.
- [12] K. Herrmann, O. Gerngross, and W. Abitz. Zur rontgenographischen Strukturforschung des gelatinemicells. *Z. Phys. Chem. B*, 10:371–394, 1930.
- [13] P. J. Flory. On the Morphology of the Crystalline State in Polymers. *Journal of the American Chemical Society*, 84(15):2857–2867, aug 1962.
- [14] P.H. Geil. Polymer single crystals (Polymer reviews, Vol. 5), P. H. Geil, Interscience, New York, 1963. *Journal of Polymer Science Part A: General Papers*, 2(4):2015–2016, apr 1964.
- [15] H. G. Zachmann. Der Einfluß der Konfigurationsentropie auf das Kristallisierungs- und Schmelzverhalten von hochpolymeren Stoffen. *Kolloid-Zeitschrift & Zeitschrift für Polymere*, 216-217(1):180–191, mar 1967.
- [16] H. G. Zachmann. Statistische Thermodynamik des Kristallisierens und Schmelzens von hochpolymeren Stoffen. *Kolloid-Zeitschrift und Zeitschrift für Polymere*, 231(1-2):504–534, may 1969.
- [17] K. H. Storks. An Electron Diffraction Examination of Some Linear High Polymers. *Journal of the American Chemical Society*, 60(8):1753–1761, aug 1938.
- [18] RALPH JACCODINE. Observations of Spiral Growth Steps in Ethylene Polymer. *Nature*, 176(4476):305–306, aug 1955.
- [19] P. H. Till. The growth of single crystals of linear polyethylene. *Journal of Polymer Science*, 24(106):301–306, apr 1957.
- [20] A. Keller. A note on single crystals in polymers: Evidence for a folded chain configuration. *Philosophical Magazine*, 2(21):1171–1175, sep 1957.
- [21] Do Y. Yoon and Paul J. Flory. Molecular morphology in semicrystalline polymers. *Faraday Discussions of the Chemical Society*, 68(0):288, jan 1979.

- [22] A. Keller. Crystalline polymers; an introduction. *Faraday Discussions of the Chemical Society*, 68(0):145, jan 1979.
- [23] Wenbing Hu. *Polymer Physics: A Molecular Approach*. 2013.
- [24] Michael Zhang, Bao-Hua Guo, and Jun Xu. *A Review on Polymer Crystallization Theories*, volume 7. 2016.
- [25] † Koji Yamada, *, ‡ Masamichi Hikosaka, ‡ Akihiko Toda, , ‡ Shinichi Yamazaki, and Katsuhiro Tagashira†. Equilibrium Melting Temperature of Isotactic Polypropylene with High Tacticity: 1. Determination by Differential Scanning Calorimetry. 2003.
- [26] J. P. Arlif, P. A. Spegt, and A. E. Skoulios. Etude de la cristallisation des polymères I. Structure lamellaire de polyoxyéthylènes de faible masse moléculaire. *Die Makromolekulare Chemie*, 99(1):160–174, dec 1966.
- [27] Yasuhiro Takahashi and Hiroyuki Tadokoro. Structural Studies of Polyethers, $(-\text{CH}_2\text{m}-\text{O}-)^n$. X. Crystal Structure of Poly(ethylene oxide). *Macromolecules*, 6(5):672–675, 1973.
- [28] A. J. Kovacs, C. Straupe, and A. Gonthier. Isothermal growth, thickening, and melting of poly(ethylene oxide) single crystals in the bulk. II. *Journal of Polymer Science: Polymer Symposia*, 59(1):31–54, mar 1977.
- [29] Dirk Pfefferkorn, Samuel O. Kyeremateng, Karsten Busse, Hans Werner Kammer, Thomas Thurn-Albrecht, and Jörg Kressler. Crystallization and melting of poly(ethylene oxide) in blends and diblock copolymers with poly(methyl acrylate). *Macromolecules*, 44(8):2953–2963, 2011.
- [30] Virgil Percec, Coleen Pugh, Oskar Nuyken, and Stephen D. Pask. Macromonomers, Oligomers and Telechelic Polymers. In *Comprehensive Polymer Science and Supplements*, pages 281–357. Elsevier, 1989.
- [31] C P Buckley and A J Kovacs. Melting behaviour of low molecular weight poly (ethylene-oxide) fractions. In *Polymere Aspekte*, pages 44–52. 1975.
- [32] Rachel Wong, Mark Ashton, and Kalliopi Dodou. Effect of Crosslinking Agent Concentration on the Properties of Unmedicated Hydrogels. *Pharmaceutics*, 7(3):305–319, sep 2015.

- [33] Wilfredo Yave, Anna Szymczyk, Nancy Yave, and Zbigniew Roslaniec. Design, synthesis, characterization and optimization of PTT-b-PEO copolymers: A new membrane material for CO₂separation. *Journal of Membrane Science*, 362(1-2):407–416, 2010.
- [34] Brian C Okerberg, Christopher L Soles, Jack F Douglas, Hyun Wook Ro, Alamgir Karim, and Daniel R Hines. Crystallization of Poly(ethylene oxide) Patterned by Nanoimprint Lithography. 2007.
- [35] Jana Herzberger, Kerstin Niederer, Hannah Pohlit, Jan Seiwert, Matthias Worm, Frederik R Wurm, and Holger Frey. Polymerization of Ethylene Oxide, Propylene Oxide, and Other Alkylene Oxides: Synthesis, Novel Polymer Architectures, and Bioconjugation. 2015.
- [36] A Marshall, R C Domszv, H H Teo, R H Mobbs, and C Booth. CRYSTALLINITY OF ETHYLENE OXIDE OLIGOMERS. *European Polymer Journal*, 17(893), 1981.
- [37] Y. Kong and Y. N. Hay. The measurement of cristalinity of polymers by DSC. *Polymer*, 43(1):3873–3878, 2002.
- [38] Leslie Lamport. *ETEX — A Document Preparation System*. Addison-Wesley, Reading, Massachusetts, second edition, 1994.